Quantum theory of terahertz emission due to ultrashort pulse ionization of gases

K. Schuh,* M. Scheller, J. Hader, and J. V. Moloney
Department of Mathematics, Arizona Center for Mathematical Sciences, University of Arizona, Tucson, Arizona 85721, USA and College of Optical Sciences, University of Arizona, Tucson, Arizona 85721, USA

S. W. Koch
College of Optical Sciences, University of Arizona, Tucson, Arizona 85721, USA and Department of Physics and Material Science Center, Philipps-University, 35032 Marburg, Germany

(Received 1 July 2013; published 5 December 2013)

A microscopic model is developed to analyze terahertz (THz) emission after ultrashort one- and two-color laser-pulse excitations of an atomic gas. Optical Bloch equations are derived to describe the pulse-induced ionization in the many-atom system including the Coulombic scattering of the ionized electrons. The model captures the continuous transition between the tunneling and the multiphoton ionization regimes. Numerical evaluations for a wide range of pulse configurations identify optimized excitation conditions for strong THz emission.

DOI: 10.1103/PhysRevE.88.063102 PACS number(s): 52.25.Os, 42.65.Ky, 52.25.Jm, 52.20.Fs

I. INTRODUCTION

Electromagnetic fields in the terahertz (THz) frequency range are of interest for a wide range of applications, including spectroscopy of organic and inorganic matter, nondestructive testing of industrial goods, all the way to homeland security [1]. The increasing availability of high-intensity THz fields even allows for the study of nonlinear phenomena [2–4].

Besides optical rectification of femtosecond laser pulses in nonlinear crystals [5–7], the THz generation in ambient air is an effective way to generate strong pulses. After the first demonstration of THz emission from a laser-induced plasma [8], it was shown that the efficiency for THz generation can significantly be enhanced through the application of an electric dc field which accelerates the photoionized electrons and, thus, induces a transient space charge separation [9]. Recently, is has been demonstrated that highly efficient THz generation can be observed if two-color laser pulses are used to create the plasma. This effect has been attributed to four-wave mixing [10–16] or temporal asymmetries in the E fields of the pulses [17–19].

In this paper, we develop a microscopic theory that allows us to systematically study THz generation in atomic plasmas. We keep our analysis as general as possible since we want to identify the mechanisms responsible for THz generation in a wide range of experimentally relevant conditions. In order to focus on the fundamental aspects, we evaluate the theory for an atomic hydrogen gas as the most simple example. Furthermore, we treat the plasma as a point source, i.e., we do not account for detector influences or geometric effects, that have been investigated, e.g., in Refs. [20–22]. For a point source, the temporal change in the current leads to a dipole emission that is proportional to the current change, which will, thus, be the focus of our analysis.

II. MODEL

For the modeling of the optical excitation, we use a generalized version of the optical Bloch equations [23]. In this semiclassical model, the optical field is described as a classical field, whereas, the electrons are treated quantum mechanically. Since we are interested in dilute gases at ambient pressure, we focus our investigations on a model system with N hydrogen atoms in the volume V. For this low-density configuration, it is well justified to neglect many-body modifications of the atomic continuum states, which can be classified by their momentum $\vec{k}$. In this aspect, our model corresponds to the strong field approximation (SFA) in plasma physics (see, e.g., Ref. [24]). Although the SFA is valid in the tunneling ionization regime, our model also captures the essential properties of the multiphoton regime. Thus, our model predicts strong photon resonances and a distinct wavelength dependency of the ionization rate as well as the appearance of momentum rings (see, e.g., Ref. [25]). For the THz-generation investigations, we need to compute the optically induced current dynamics in the system. Since the bound states influence the polarization and current only at higher frequencies, they are not relevant in the THz regime, and it is sufficient to limit our calculation to the hydrogen ground state $1s$ and the continuum states. The omission of the intermediate states leads to a significantly reduced ionization degree. Compared with H atoms [26], our simplified system requires an about sixfold increased intensity to realize the same degree of ionization. We compensate for this shortcoming by using appropriately chosen higher intensities.

The noninteracting part of the Hamiltonian is

$$H_0 = \sum_s \epsilon_s a_s^\dagger a_s + \sum_{\vec{k}} \epsilon_{\vec{k}} a_{\vec{k}}^\dagger a_{\vec{k}}, \tag{1}$$

where $a^\dagger$ and a are the electron creation and annihilation operators. The transitions of electrons from the bound to a continuum state are treated in dipole approximation (see, e.g., Ref. [27]). The acceleration of free electrons in an E field leads to an additional gradient term in the Hamiltonian,

$$H_D = -\frac{e}{\hbar}\vec{E}(t)\vec{\nabla}_{\vec{k}} - \sum_{s\vec{k}} \Omega_{s\vec{k}}(t) a_s^\dagger a_{\vec{k}} + \Omega_{\vec{k}s}(t) a_{\vec{k}}^\dagger a_s. \tag{2}$$

The Rabi frequency is

$$\Omega_{s\vec{k}}(t) = \vec{d}_{s\vec{k}}\vec{E}_C(t), \tag{3}$$

*kschuh@optics.arizona.edu

where e is the elementary charge, $\vec{E}$ is the physical E field, and $\vec{E}_C$ is the complex E field, respectively. In our evaluations, we assume a linear field polarization. The dipole matrix elements $\vec{d}_{s\vec{k}} = \langle \Phi_s | - e\vec{r} | \Phi_{\vec{k}} \rangle$ determining the strength of the respective transitions decay for large momenta k. Altogether, our model describes the multiphoton as well as the tunneling ionization regimes [28] and allows for arbitrary pulse shapes.

Evaluating the Heisenberg equations of motion, we obtain, for the populations of the ground state $f_s = \langle a_s^\dagger a_s \rangle$, the continuum states $f_{\vec{k}} = \langle a_{\vec{k}}^\dagger a_{\vec{k}} \rangle$, and the microscopic polarizations (transition amplitudes) $P_{s\vec{k}} = \langle a_s^\dagger a_{\vec{k}} \rangle$,

$$i\hbar \frac{d}{dt} P_{s\vec{k}} = [\epsilon_s - \epsilon_{\vec{k}}] P_{s\vec{k}} + \Omega^*_{s\vec{k}} [f_{\vec{k}} - f_s] - \frac{e}{\hbar} \vec{\nabla}_{\vec{k}} P_{s\vec{k}} \vec{E}, \quad (4)$$

$$i\hbar \frac{d}{dt} f_s = \sum_{\vec{k}} \Omega^*_{s\vec{k}} P^*_{s\vec{k}} - \Omega_{s\vec{k}} P_{s\vec{k}}, \quad (5)$$

$$i\hbar \frac{d}{dt} f_{\vec{k}} = N[\Omega_{s\vec{k}} P_{s\vec{k}} - \Omega^*_{s\vec{k}} P^*_{s\vec{k}}] - \frac{e}{\hbar} \vec{\nabla}_{\vec{k}} f_{\vec{k}} \vec{E}. \quad (6)$$

The atoms are treated as a homogeneous density with the consequence that the expectation values for all atoms are equal, and the sum over them simply yields the atom number N. Since we evaluate the theory in the continuum limit, at the end, only the density of atoms is of importance.

So far, we have not included dissipative or damping terms. However, it is well known that the current decay contributes to the THz emission [29,30]. In our model, the dominant contribution for this decay comes from the Coulomb electron-ion collisions. The additional electron-electron interaction does not influence the current directly since momentum conservation leads to current conservation in the case of uniform charge to mass ratios. We are also neglecting other collective processes that influence the efficiency and spectral details of the THz emission, i.e., plasma oscillations, electron-neutral collisions, and geometric effects that have been studied, e.g., in Refs. [31,32].

Ignoring the backaction of the electrons on the heavy ions, we model the electron-ion collisions via the single-particle Hamiltonian,

$$H_{\text{el-ion}} = -\sum_{\vec{k}\vec{k}'} a_{\vec{k}}^\dagger a_{\vec{k}'} W(|\vec{k}' - \vec{k}|). \quad (7)$$

Here, we include only the continuum-state electrons since the multiatom modifications of the single-atom bound electrons are negligible in a dilute gas. For the interaction, we use a screened Coulomb potential,

$$W(q) = \frac{1}{V} \frac{e^2}{\epsilon_0 (q^2 + \kappa^2)}, \quad (8)$$

with the permittivity ϵ_0 and treat the screening within the Debye-Hückel approximation [23]. This leads to an inverse screening length,

$$\kappa = \sqrt{\frac{4\pi e^2}{\epsilon_0} \rho \beta}, \quad (9)$$

that depends on the reciprocal of the thermodynamic temperature β and the electron density ρ. Since this value changes during the optical excitation, κ is also time dependent.

Evaluating the Heisenberg equation of motion due to the electron-ion Hamiltonian (7) and implementing the second Born Markov approximation [23], we obtain

$$\left. \frac{df_{\vec{k}}(t)}{dt} \right|_{\text{el-ion}} = -N_{\text{ion}} \frac{2\pi}{\hbar} \sum_{\vec{k}'} \delta(\epsilon_{\vec{k}} - \epsilon_{\vec{k}'}) \times W^2(|\vec{k}' - \vec{k}|)[f_{\vec{k}}(t) - f_{\vec{k}'}(t)] \quad (10)$$

where N_{ion} is the number of ions and multiple-ion scattering effects have been neglected. With this ansatz for the electron-ion scattering, we ignore the influence of the free-electron acceleration during the pulse, e.g., the inverse bremsstrahlung. In the numerical evaluation, Eq. (10) has to be added to the optical part Eq. (6).

III. NUMERICAL EVALUATION

We solve the coupled differential equations (4)–(6) and (10) by using the fourth-order Runge-Kutta method. The summations over the continuum states $\vec{k}$ are solved in the continuum limit, i.e., $\sum_{\vec{k}} \to \frac{V}{(2\pi)^3} \int dk^3$. First, we study the optically induced ionization dynamics for high-intensity femtosecond pulse excitation with a peak intensity of 6×10^{18} W/m^2. We analyze the system response to excitation pulses with one- or two-color carrier waves. In all cases, we choose the fundamental frequency as $\hbar\omega = 1.5$ eV (equals 827 nm and 363 THz). In the discussion, we refer to this part as the *first harmonic component*. For the two-color pulses, we add a frequency doubled contribution, the *second harmonic component*, whose amplitude is chosen as 1/3 of the first harmonic component. Since the two-color pulses are sensitive to the phase difference between both components, we investigate the extreme cases where the phases of the first and second harmonics either match at the pulse center or where they differ by $\pi/2$. Pulses of this kind are of practical importance since they can easily be created by second harmonic generation and their relative phase can be adjusted precisely by exploiting the wavelength dispersion in air [17].

Choosing 15 fs (FWHM) Gaussian excitation pulses, we obtain the ionization dynamics shown in Fig. 1. We notice a steplike carrier ionization with the largest increase occurring close to the pulse extrema. During each cycle of the one-color pulse (left panels in Fig. 2), we have two equidistant ionization steps resulting from the symmetric positive and negative field-amplitude parts in each cycle.

Due to its much larger positive than negative field amplitudes, the in-phase two-color pulse (middle panels in Fig. 2) shows only one pronounced ionization step per cycle. The ionization change due to the negative pulse peaks is significantly smaller. However, as we can see in Fig. 1, the total ionization is significantly enhanced relative to the same energy one-color pulse due to the larger positive field amplitudes in combination with the strong nonlinearities.

The two-color pulse with a $\pi/2$-phase difference (right panels in Figs. 1 and 2) is asymmetric in time. The center peak of the E field is shifted by 0.19 fs relative to the center of the pulse envelope. Furthermore, the time between a field maximum and the next field minimum is significantly shorter (44%) than that between a minimum and the following

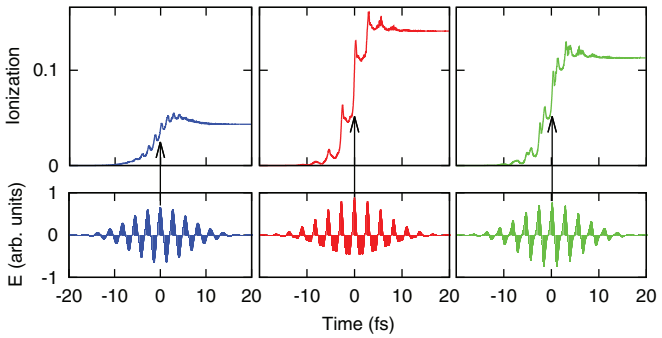

FIG. 1. (Color online) Resulting time evolution of the carrier ionization (upper part) for different 15 fs Gaussian excitation pulses shown in the respective lower parts. The results for a one-color pulse are plotted in the left panels, those for the in-phase two-color pulse are plotted in the middle panels, and those for the two-color pulse with a $\pi/2$-phase difference are plotted in the right panels, respectively. In all cases, we choose the peak intensity of the fundamental carrier wave as 6×10^{18} W/m^2.

maximum. Therefore, we always observe pairs of ionization steps bunched together.

According to Maxwell's equations, the generation of electromagnetic radiation is linked directly to the temporal changes in the current density,

$$\vec{j}(t) = \frac{1}{V} \sum_{\vec{k}} f_{\vec{k}}(t) \vec{k} \frac{e\hbar}{m}. \tag{11}$$

To study the generation of THz fields, we evaluate the current change in frequency space,

$$c(\nu) = \int dt\, e^{2\pi i \nu t} \frac{d j_z(t)}{dt}, \tag{12}$$

where we assumed a linearly polarized E field such that only the component j_z is finite.

Figure 3 shows the absolute value of the computed current change for a peak intensity of 6×10^{18} W/m^2 in the first harmonic component. For all three excitation pulses, we notice a dominant peak in the spectra at the fundamental frequency (363 THz) that is caused by the acceleration of the freed electrons oscillating with the field frequency. In the region below the fundamental frequency, the current change is monotonically decreasing in the case of the one-color pulse

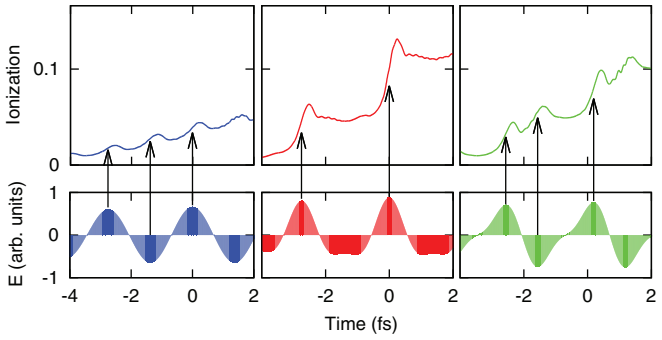

FIG. 2. (Color online) Magnification of Fig. 1: The arrows indicate the alignment of the pulse peaks with the periods of rapid ionization.

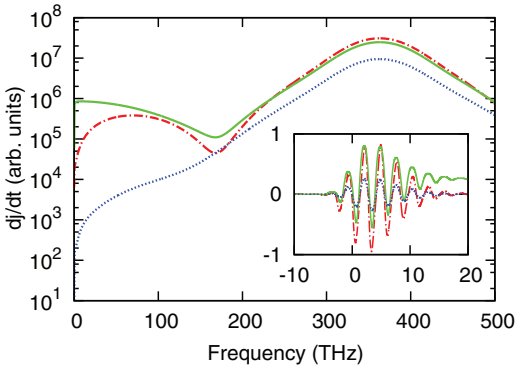

FIG. 3. (Color online) Frequency spectrum of the current change, Eq. (12), induced by the one-color pulse (blue dotted curve), by the two-color pulse with in-phase components (red dot-dashed curve), and by the two color-pulse with a $\pi/2$-phase difference (green solid curve). In all cases, the peak intensity of the first harmonic component is 6×10^{18} W/m^2, and the pulse duration is 15 fs. The inset shows the corresponding currents (in arb. units) as a function of time (in femtoseconds).

excitation (blue dotted curve). For the two-color pulse with matched phases (red dot-dashed curve), we also notice a declining current change below 75 THz. In contrast, the two-color pulse with a $\pi/2$-phase difference (green solid curve) yields a current change that increases for small frequencies and shows a wide slowly decaying plateau with a maximum at 8 THz. The numerical value of the current change at 1 THz is above 90% of the maximum, and at 0.1 THz, it is still 50%, respectively. For the high field intensity studied here, this pulse shape is, thus, most efficient in the generation of low THz-frequency components.

The current generation dynamics is shown in the inset of Fig. 3. In addition to the instantaneous high-frequency current contributions, we notice some residual quasi-dc current after the pulse. This current decays on a picosecond time scale due to the damping by the electron-ion interaction. This slowly decaying current part is responsible for the low-frequency contributions in the spectra.

To gain a better understanding of the excitation conditions needed for efficient THz generation, we first focus on the symmetry properties of the excitation pulses. Due to the strong nonlinearity of the process, most electrons are ionized at times close to the extrema of the exciting E field; compare Fig. 2. The induced current after the pulse is then proportional to the freed electron's acceleration during the remaining pulse, i.e.,

$$j_z^R(t) = \frac{e^2}{m} \int_t^\infty dt' E_z(t'). \tag{13}$$

For illustration purposes, we discuss the current generation due to artificial pulses consisting of linear segments representing 1.5 field cycles, see the top panels in Fig. 4. Even though such pulses are not realistic, they possess the same basic symmetries as the investigated Gaussian pulses (shown in Fig. 1) and allow for a simple analysis.

The bottom panels of Fig. 4 show $j_z^R(t)$ (solid curves) induced by the corresponding pulses in the top panels. Assuming a stepwise electron ionization at each field extremum, the respective contribution to the quasi-dc current is given by

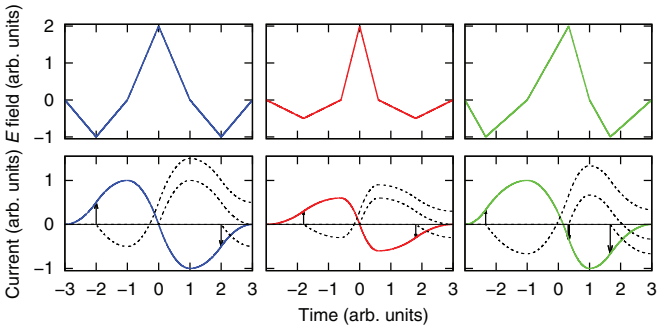

FIG. 4. (Color online) Simplified model pulses (upper panels) and the resulting current $j_z^R(t)$ (with $e = m = 1$) at the end of the pulse for an electron ionized at the time t (lower panels, solid curves). The time evolution of the current components due to one electron ionized at a field extremum (marked by the arrows) is shown as dashed curves. All quantities are presented in dimensionless units; see the text for details.

the value of $j_z^R(t_{\rm extr})$ at the time $t_{\rm extr}$ of the extremum multiplied by the number of electrons freed at the corresponding peak.

For the one-color pulse (left panels in Fig. 4), the first peak ($t = -2$) yields a positive contribution to the quasi-dc current (the value of the solid curve is indicated by the first arrow in the lower panel). The dashed curve shows the evolution of the current per electron ionized at this time; its value after the pulse is identical to that of the solid curve marked by the arrow. The other dashed curves show the analogous scenario for the later peaks. We see that, for the central peak, $j_z^R(t)$ vanishes, indicating a zero contributed to the total quasi-dc current. The third and last peak causes a negative contribution that neutralizes the contribution of the first peak since both peaks have the same amplitude. As a consequence, this symmetric pulse shape does not create a quasi-dc current under these conditions.

The same is true for the in-phase two-color pulses (middle panels in Fig. 4). In contrast, the two-color pulse with a $\pi/2$-phase difference (right panels) produces a quasi-dc current since the main peak as well as the combination of the two other peaks create a finite net current determined by the remaining acceleration $j_z^R(t)$ after the pulse. Similar features have been discussed for two-color pulses by Kim *et al.* [17] and Wang *et al.* [18].

Besides the pulse shape, the intrinsic dynamics of the electronic system also contributes to the overall asymmetry of the quasi-dc current generation process. As can be seen in Fig. 2, the ionization maximizes not exactly at the time of the field extrema but shortly thereafter. Furthermore, the process is partially reversed by the subsequently decreasing driving field. These features are an indication that the system is close to the ultrafast adiabatic following regime [33]. Thus, symmetrically shaped pulses also induce a finite current, which is, however, significantly smaller than for the asymmetric pulse shapes. In the context of the simplified pulses in Fig. 4, this can be described as an effective shift in the ionization times. This time shift leads to a change in the resulting quasi-dc current in the direction opposite to the E field at the creation time. Even if there are negative and positive contributions, the highly nonlinear impact of the amplitude on the ionization rate leads to a remaining net contribution to the resulting current. In comparison to the one-color pulse, this contribution is significantly larger for the two-color in-phase configuration (middle panels) since the positive amplitudes are much larger than the negative ones. The combined influence of the original pulse asymmetry with this electron-dynamics-induced asymmetry is referred to as "effective asymmetry."

Returning to the analysis of the THz generation by the more realistic Gaussian shaped pulses, we introduce the averaged induced current change rates up to 2.25 THz,

$$C_{2\ \rm THz} = \frac{1}{2.25\ \rm THz}\int_0^{2.25\ \rm THz} d\nu\, c(\nu), \tag{14}$$

and up to 50.25 THz,

$$C_{50\ \rm THz} = \frac{1}{50.25\ \rm THz}\int_0^{50.25\ \rm THz} d\nu\, c(\nu). \tag{15}$$

For the idealized case of a point source, these rates are proportional to the emitted far-field THz signal in the spectral range up to 2.25 THz, respectively, 50.25 THz. In an experiment, the 2.25 THz range could be measured, e.g., by a ZnTe detector (see, e.g., Ref. [12]).

Figure 5 shows the computed $C_{2\ \rm THz}$ for different peak intensities of the excitation pulses shown in Fig. 1. As mentioned before, we have to choose rather high intensities to reach a given ionization degree since we omit the intermediate bound states. As we can see, the 15 fs FWHM one-color pulse (blue stars) is significantly less efficient for THz generation than the two-color pulses (red crosses and green × symbols). Even if the rate increases very fast above the ionization threshold (around 1×10^{18} W/m^2), it always remains smaller than that of the two-color pulses due to their higher effective asymmetry.

The impact of this asymmetry increases linearly with the amplitude E_ω (for a given $E_\omega/E_{2\omega}$) and the density of ionized electrons I. Thus, one can fit this "asymmetry

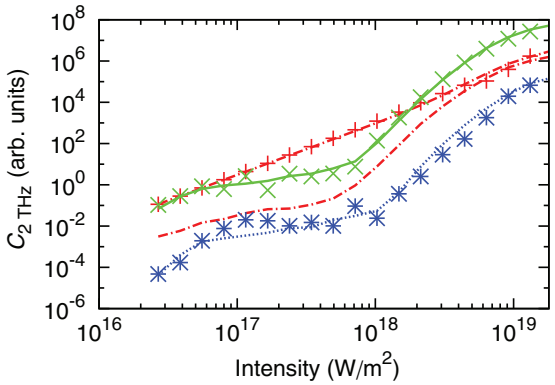

FIG. 5. (Color online) Calculated values of $C_{2\ \rm THz}$, Eq. (14), for the Gaussian 15 fs pulses shown in Fig. 1 (one-color blue stars, two-color in-phase red crosses, and $\pi/2$-phase difference green × symbols). The simplified fits of the low THz current change rate for the one-color pulse are shown as the blue dotted curve and, for the two-color pulse with a $\pi/2$-phase difference, as the green solid curve, respectively. The results for the two-color in-phase pulse are plotted as red dot-dashed curves with (upper curve) and without (lower curve) the four-wave mixing contribution.

contribution" as

$$C^{\text{asym}}_{2\,\text{THz}} \propto A_{2\,\text{THz}} I E_\omega. \tag{16}$$

Since this contribution is dependent on the pulse shapes, we introduce a pulse-shape efficiency factor $A_{2\,\text{THz}}$. This factor is defined as the ratio of current change per ionized electron due to effective asymmetry in a given frequency range to the corresponding value of the one-color pulse with the same amplitude of the first harmonic. Numerically, $A_{2\,\text{THz}}$ is obtained by fitting to the calculated values of $C_{2\,\text{THz}}$ (lines) subtracting the further subsequently discussed contributions.

Relative to the one-color case (blue dotted curve in Fig. 5), the effective asymmetry is ten times larger for the two-color in-phase pulse (lower red dot-dashed curve). The asymmetrically shaped two-color pulses with a $\pi/2$-phase difference (green solid curve) even yield a 330 times larger effective asymmetry. Thus, they are most efficient in the creation of $C_{2\,\text{THz}}$ at the high intensities used in Figs. 1–3.

The comparison with the full numerical results in Fig. 5 shows that the asymmetry contributions alone do not explain the behavior of the THz-generation rate. In fact, at medium low intensities, the in-phase two-color pulses (red crosses) are equally or even more efficient than the phase-shifted ones (green $\times$ symbols). This regime is interesting for filamentation studies, see, e.g., Refs. [21,34].

To identify the origin for this difference, we analyze the effect of plasma assisted four-wave mixing. Here, the pulse created plasma supports four-wave mixing between frequency components of the same pulse. In particular, the mixing of two photons with frequencies close to ω and one close to 2ω can result in the generation of low-frequency photons in the THz range. Since this process does not require a residual ionization, even temporarily freed electrons are contributing.

As long as $E_\omega \gg E_{2\omega}$, the amount of temporal plasma density is proportional to the first harmonic intensity ($\propto E^2_\omega$). The four-wave mixing itself is then proportional to $\propto E^2_\omega E_{2\omega}$, where $E_{2\omega}$ is the amplitude of the second harmonic. Thus, the total four-wave-mixing contribution should scale like

$$C^{\text{four wave}}_{\text{THz}} \propto E^4_\omega E_{2\omega}. \tag{17}$$

The upper red dot-dashed line in Fig. 5 shows $C^{\text{four wave}}_{\text{THz}} + C^{\text{asym}}_{\text{THz}}$. In reality, these contributions are not simply additive since they may possess different phases. However, as we can already see from our simple estimate, the four-wave-mixing part is the dominant source for the generation of THz radiation for in-phase two-color pulses at low and medium intensities. This effect plays no role for the phase-shifted pulses since the phase difference of the spectral components inhibits efficient four-wave mixing in this case [17].

The situation changes only slightly for $C_{50\,\text{THz}}$ as shown in Fig. 6. Since transient ionization contributions can be expected in this regime, we analyze the contribution,

$$C^{\text{temp}}_{\text{THz}} \propto A_{\text{temp}} E^3_\omega, \tag{18}$$

where A_{temp} is the temporal pulse-shape efficiency coefficient. The factor E^2_ω accounts for the instantaneous plasma density, and the asymmetry is proportional to E_ω. This transient effect only leads to a short current that is far weaker than the current due to the long lasting residual ionization and is, thus, relevant only well below the ionization threshold. Furthermore, this

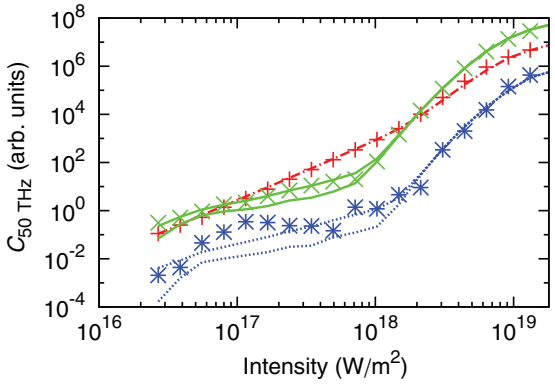

FIG. 6. (Color online) The same as Fig. 5, however, for $C_{50\,\text{THz}}$. The fits for the one-color pulse (blue dotted curve) and the two-color phase-shifted pulse (green solid curve) include (upper curves) or exclude (lower curves) the contribution $C^{\text{temp}}_{\text{THz}}$ that arises from a temporal plasma at low intensities (see the text).

contribution is significantly smaller than the four-wave-mixing part and is, thus, negligible for the in-phase two-color case (red symbols in Fig. 6). In contrast, it leads to an increased efficiency at low to medium intensities, both for the one-color and the two-color pulses with a $\pi/2$-phase difference below the ionization threshold.

In addition to the intensity dependence, it is interesting to study the influence of the pulse length on the THz-generation process. Figure 7 summarizes the computed results for $C_{2\,\text{THz}}$ as a function of the pulse length for the fixed pulse energy, i.e., the product of the pulse length and peak intensity is constant. In all cases, shorter pulses are significantly more efficient for THz generation than longer ones. For the one-color case (blue stars) and the two-color in-phase case (red crosses), we can identify a "short-pulse" contribution approximated by

$$C^{\text{short}}_{\text{THz}} \propto I^3 E_\omega. \tag{19}$$

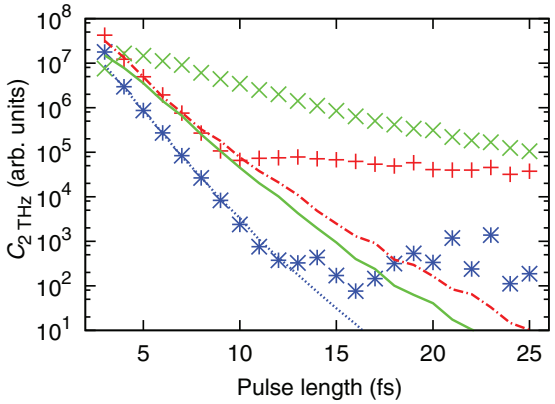

FIG. 7. (Color online) THz current change rate $C_{2\,\text{THz}}$ as a function of the pulse length for Gaussian pulses. The 15 fs results correspond to the pulses shown in Fig. 1. The computed results for the one-color pulse are shown as blue stars, those for the in-phase two-color pulse are plotted as red crosses, and those for the two-color pulse with the $\pi/2$-phase difference are represented by the green $\times$ symbols, respectively. In all cases, the pulse energy is constant, i.e., the intensity increases with decreasing pulse length. The fit lines show the short-pulse approximation discussed in the text.

Although this is the dominant source of $C_{2\,\mathrm{THz}}$ for pulse lengths less than 10 fs in the one-color (blue dotted curve) and two-color in-phase case (red dot-dashed curve), it is in the two-color $\pi/2$-phase difference case (green solid curve) neglectable for pulse lengths of more than 4 fs. Nevertheless, the THz emission profits in the last case from an increasing ionization as well as an increasing E-field amplitude that increases $C_{2\,\mathrm{THz}}^{\mathrm{asym}}$. Our calculations for the one-color case are in qualitative agreement with previous studies [32,35].

IV. CONCLUSION

To summarize, we present a consistent microscopic theory for short-pulse ionization of atomic gases and the effects of pulse-induced generation of THz radiation. We identify plasma assisted four-wave mixing of frequency components within one pulse as the dominant source for THz generation at intensities below the ionization threshold and at low ionization, which is the regime of most filamentation studies. For higher intensities, pulse-symmetry effects are the dominant favoring asymmetric pulse shapes. Due to the electron dynamics, symmetric pulses also lead to an asymmetric excitation. However, the generated THz signals due to this effect are at least one order of magnitude smaller. Although two-color pulses with an optimized phase relation and a pulse length of more than 5 fs produce significantly more THz than one-color pulses in the regime of 3–4 fs pulses, the actual pulse shape (one color, two color) only has a small influence on the efficiency of the THz emission. In combination with high intensity, short pulses turn out to be the most efficient.

ACKNOWLEDGMENTS

We acknowledge financial support through the AFOSR MURI "Mathematical Modeling and Experimental Validation of Ultrafast Nonlinear Light-Matter Coupling associated with Filamentation in Transparent Media," Grant No. FA9550-10-1-0561 and partial support through AFOSR Grant No. FA9550-10-1-0064.

[1] P. U. Jepsen, D. G. Cooke, and M. Koch, Laser Photonics Rev. **5**, 124 (2011).
[2] H. Hirori, M. Nagai, and K. Tanaka, Phys. Rev. B **81**, 081305 (2010).
[3] M. C. Hoffmann, J. Hebling, H. Y. Hwang, K.-L. Yeh, and K. A. Nelson, Phys. Rev. B **79**, 161201 (2009).
[4] S. Leinß, T. Kampfrath, K. v. Volkmann, M. Wolf, J. T. Steiner, M. Kira, S. W. Koch, A. Leitenstorfer, and R. Huber, Phys. Rev. Lett. **101**, 246401 (2008).
[5] R. Huber, A. Brodschelm, F. Tauser, and A. Leitenstorfer, Appl. Phys. Lett. **76**, 3191 (2000).
[6] C. Kübler, R. Huber, and A. Leitenstorfer, Semicond. Sci. Technol. **20**, S128 (2005).
[7] H. Hirori, F. Blanchard, K. Tanaka *et al.*, Appl. Phys. Lett. **98**, 091106 (2011).
[8] H. Hamster, A. Sullivan, S. Gordon, W. White, and R. W. Falcone, Phys. Rev. Lett. **71**, 2725 (1993).
[9] T. Loffler, F. Jacob, and H. Roskos, Appl. Phys. Lett. **77**, 453 (2000).
[10] X. Xie, J. Dai, and X.-C. Zhang, Phys. Rev. Lett. **96**, 075005 (2006).
[11] J. Peñano, P. Sprangle, B. Hafizi, D. Gordon, and P. Serafim, Phys. Rev. E **81**, 026407 (2010).
[12] D. Cook and R. Hochstrasser, Opt. Lett. **25**, 1210 (2000).
[13] M. Kress, T. Löffler, S. Eden, M. Thomson, and H. G. Roskos, Opt. Lett. **29**, 1120 (2004).
[14] T. Bartel, P. Gaal, K. Reimann, M. Woerner, and T. Elsaesser, Opt. Lett. **30**, 2805 (2005).
[15] M. D. Thomson, V. Blank, and H. G. Roskos, Opt. Express **18**, 23173 (2010).
[16] H. Roskos, M. Thomson, M. Kreß, and T. Löffler, Laser Photonics Rev. **1**, 349 (2007).
[17] K.-Y. Kim, J. H. Glownia, A. J. Taylor, and G. Rodriguez, Opt. Express **15**, 4577 (2007).
[18] W.-M. Wang, Y.-T. Li, Z.-M. Sheng, X. Lu, and J. Zhang, Phys. Rev. E **87**, 033108 (2013).
[19] J. Dai, N. Karpowicz, and X.-C. Zhang, Phys. Rev. Lett. **103**, 023001 (2009).
[20] C. D'Amico, A. Houard, M. Franco, B. Prade, A. Mysyrowicz, A. Couairon, and V. T. Tikhonchuk, Phys. Rev. Lett. **98**, 235002 (2007).
[21] Y. S. You, T. I. Oh, and K. Y. Kim, Phys. Rev. Lett. **109**, 183902 (2012).
[22] C. Amico, A. Houard, S. Akturk, Y. Liu, J. Le Bloas, M. Franco, B. Prade, A. Couairon, V. Tikhonchuk, and A. Mysyrowicz, New J. Phys. **10**, 013015 (2008).
[23] H. Haug and S. W. Koch, *Quantum Theory of the Optical and Electronic Properties of Semiconductors* (World Scientific, Singapore, 2004).
[24] D. Bauer, D. B. Milošević, and W. Becker, Phys. Rev. A **72**, 023415 (2005).
[25] M. Wickenhauser, X. M. Tong, D. G. Arbó, J. Burgdörfer, and C. D. Lin, Phys. Rev. A **74**, 041402(R) (2006).
[26] X. Tong and C. Lin, J. Phys. B **38**, 2593 (2005).
[27] W. Schäfer and M. Wegener, *Semiconductor Optics and Transport Phenomena* (Springer, Berlin, 2002).
[28] L. V. Keldysh, Sov. Phys. JETP **20**, 1307 (1965).
[29] N. Karpowicz and X.-C. Zhang, Phys. Rev. Lett. **102**, 093001 (2009).
[30] V. Kostin and N. Vvedenskii, Opt. Lett. **35**, 247 (2010).
[31] A. Bystrov, N. Vvedenskii, and V. B. Gildenburg, JETP Lett. **82**, 753 (2005).
[32] V. B. Gildenburg and N. V. Vvedenskii, Phys. Rev. Lett. **98**, 245002 (2007).
[33] R. Binder, S. W. Koch, M. Lindberg, N. Peyghambarian, and W. Schäfer, Phys. Rev. Lett. **65**, 899 (1990).
[34] S. Tzortzakis, G. Méchain, G. Patalano, Y.-B. André, B. Prade, M. Franco, A. Mysyrowicz, J.-M. Munier, M. Gheudin, G. Beaudin *et al.*, Opt. Lett. **27**, 1944 (2002).
[35] A. A. Silaev and N. V. Vvedenskii, Phys. Rev. Lett. **102**, 115005 (2009).